ADVANCED MATERIALS

Supporting Information

for *Adv. Mater.,* DOI: 10.1002/adma.202105199

Synergistic Integration of Chemo-Resistive and SERS Sensing for Label-Free Multiplex Gas Detection

*Hyeuk Jin Han, Seunghee H. Cho, Sangjun Han, Ji-Soo Jang, Gyu Rac Lee, Eugene N. Cho, Sang-Joon Kim, Il-Doo Kim, Min Seok Jang, Harry L. Tuller, Judy J. Cha, and Yeon Sik Jung**

Supporting Information

Synergistic Integration of Chemo-resistive and SERS Sensing for Label-Free Multiplex Gas Detection

Hyeuk Jin Han,[¶] Seunghee H. Cho,[¶] Sangjun Han, Ji-Soo Jang, Gyu Rac Lee, Eugene N. Cho, Sang-Joon Kim, Il-Doo Kim, Min Seok Jang, Harry L. Tuller, Judy J. Cha, and Yeon Sik Jung*

[¶] These authors contributed equally to this work.

Dr. H. J. Han, S. H. Cho, Dr. J.-S. Jang, G. R. Lee, Dr. E. N. Cho, Prof. I.-D. Kim, Prof. Y. S. Jung
Department of Materials Science and Engineering, Korea Advanced Institute of Science and Technology (KAIST), 291 Daehak-ro, Yuseong-gu, Daejeon 34141, Republic of Korea
Dr. H. J. Han, Prof. J. J. Cha
Department of Mechanical Engineering and Materials Science, Yale University, New Haven, CT 06511, USA
Dr. H. J. Han, Prof. J. J. Cha
Energy Sciences Institute, Yale West Campus, West Haven, CT 06516, USA
S. Han, Prof. M. S. Jang
School of Electrical Engineering, Korea Advanced Institute of Science and Technology (KAIST), 291 Daehak-ro, Yuseong-gu, Daejeon 34141, 34141, Republic of Korea
Dr. S.-J. Kim, Prof. H. L. Tuller
Department of Materials Science and Engineering, Massachusetts Institute of Technology, Cambridge, MA, 02139, USA

E-mail: ysjung@kaist.ac.kr

Keywords: multimodal, gas sensors, nanoarchitectures, metal oxides, plasmonic metals, nano-transfer printing

Calculation of areal density of dye molecules

R6G solution (27 μL) was uniformly drop-casted on the whole surface of the substrate with an area of 1 cm^2. After drying the solvent, the average area density of the R6G molecules on the substrate was calculated according to the following equation.

$$\text{Average area density of R6G} = cNV/A \quad (1)$$

In Equation 1, c, N, V, and A indicate the molar concentration of R6G in the solution, Avogadro's number, the volume of the solution drop, and the surface area of the SERS substrate, respectively. For example, if c is 10^{-11} M, the average area density is 1.6 molecules/μm^2. In other words, fewer than two molecules exist within the Raman laser spot size (= 1 μm^2), which means nearly single-molecule detection capability could be confirmed.

Calculation of average enhancement factor (AEF)

For the experimental determination of the AEF, we compared the SERS signals from the same structure with those of ordinary Raman signals of target molecules without a SERS effect. To obtain the Raman signals as a reference, R6G solution was drop casted on a Si substrate to form a R6G film. The average enhancement factor (AEF) can then be estimated using the following equation.[1, 2]

$$\text{AEF} = (I_{\text{SERS}} \times N_{\text{Film}}) / (I_{\text{Normal}} \times N_{\text{SERS}}) \quad (2)$$

In Equation 2, where I_{SERS}, N_{Film}, N_{SERS}, and I_{Normal} represent the intensity of the SERS signal, the number of molecules of the R6G film on the Si wafer, the intensity of the Raman signal, and the number of molecules on the SERS substrate, respectively. N_{SERS} corresponds to the area density (molecules/μm^2) of the molecules, as defined above.

N_{Film} was calculated based on the following equation. A high-concentration R6G solution (10^{-3} M) was dropped on the substrate to form a thin R6G film. We then used the height of

the film, as we reported in a previous paper[1]. N_{Film} is defined as the area molecule density (molecules/μm^2) of the film, and can be calculated as the following.

$$\text{Area density of R6G} = hd\text{MN} \quad (3)$$

In Equation 3, where *h*, *d*, M, and N are the height of the film, the density of solid R6G, the molecular weight of R6G (g/mole), and Avogadro's number, respectively. In this measurement, Raman spectra for R6G films were obtained with the same signal acquisition conditions.

Calculation of composition ratio in gas mixtures

For the experimental determination of the gas composition ratio, we used SERS signals obtained with the 3D cross-point multifunctional architecture (3D-CMA) as a Raman signal amplifier. As reported in previous papers,[3-5] the relationship between SERS intensity and concentration can be expressed by the following.

$$I \propto \log C \quad (4)$$

where I is the intensity of SERS and C is the concentration of target molecules. As previously reported,[5, 6] the intensity responds independently to various targets. Therefore, for example, when two target molecules 1 and 2 are placed on the surface, the intensity of each target molecule can be expressed as

$$I_{1,\text{mix}} = k_1 \bullet \log C_1 + A_1 \quad (5)$$

$$I_{2,\text{mix}} = k_2 \bullet \log C_2 + A_2 \quad (6)$$

where k is the coefficient of proportionality between intensity and the logarithm of concentration and A_1 and A_2 are y-intercepts. To compare the concentration of each gas, intensity (I_N) can be divided by each coefficient (slope, k). For example, in the case of target molecule 1, the equation can be rearranged as

$$I_{N,1} = I_1 / k_1 = \log C_1 + A_1 / k_1 \quad (7)$$

and that for molecule 2 can be expressed as

$$I_{N,2} = I_2 / k_2 = \log C_2 + A_2 / k_2 \quad (8)$$

From these relationships, we could confirm that the difference in the normalized intensities shows a linear relationship in the log of concentration ratio, as expressed by

$$\Delta I_R = I_{N,1} - I_{N,2} = \log(C_1/C_2) + A_1/k_1 - A_2/k_2 \quad (9)$$

As a result, the ratio in the mixed gas can be calculated by each gas SERS intensity. To reduce the error of ratio calculation, we assumed the gas does not exist when the SERS intensity value is close to the value of baseline ± 5 %.

Superposition of response calculation under mixed gases

To calculate the specific concentration of mixed gases, we use the electrical response of MOS gas sensors. As reported in previous papers,[7, 8] when the MOS gas sensor is placed in mixed gases, we could approximate the total concentration change of the adsorbed oxygen ions on the surface. For example, when two gases 1 and 2 are placed in an environment, the relationship can be expressed as

$$\Delta N = k_1 C_1 + k_2 C_2 \quad (10)$$

where ΔN is the concentration change of the adsorbed oxygen ions on the surface, k is the coefficient factor of adsorption, and C is the concentration of gas. The concentration change of surface ionosorbed oxygen ions is related to the conductance (G) as follows:

$$G = G_0 + m\Delta N \quad (11)$$

where G_0 is the baseline conductance (i.e. air) and m is the conductance dependent on the sensing material. In terms of the response (R) of mixed gases, the relationship can be written as

$$R_{mix} = G/G_0 = 1 + k'_1 C_1 + k'_2 C_2 \quad (12)$$

However, when the sensor is exposed to low concentrations (under hundred p.p.m level), the response can be approximated as a linear relationship: $R=1+kC$.[7-9] Therefore, if we could obtain the responses for various gases independently, the total response of the sensor in mixed gases could be expressed as follows:

$$R_{mix} = 1 + (R_1 - 1) + (R_2 - 1) \quad (13)$$

For example, based on the single component analysis in Figure 5b, the response of nitrobenzene and toluene at 50 ppm was 11.3 and 8.0, respectively. By calculation of the mixed gas response based on a single component analysis, the mixed gas response should be 18.3. In fact, when placed in a gas mixture consisting of toluene and nitrobenzene at a ratio of 50:50, the MOS gas sensor shows a similar response of 18.5, as shown in Figure 5a. This information combined with the electrical response data enable the deduction of the individual concentration of mixed gases, as shown in Figure S20.

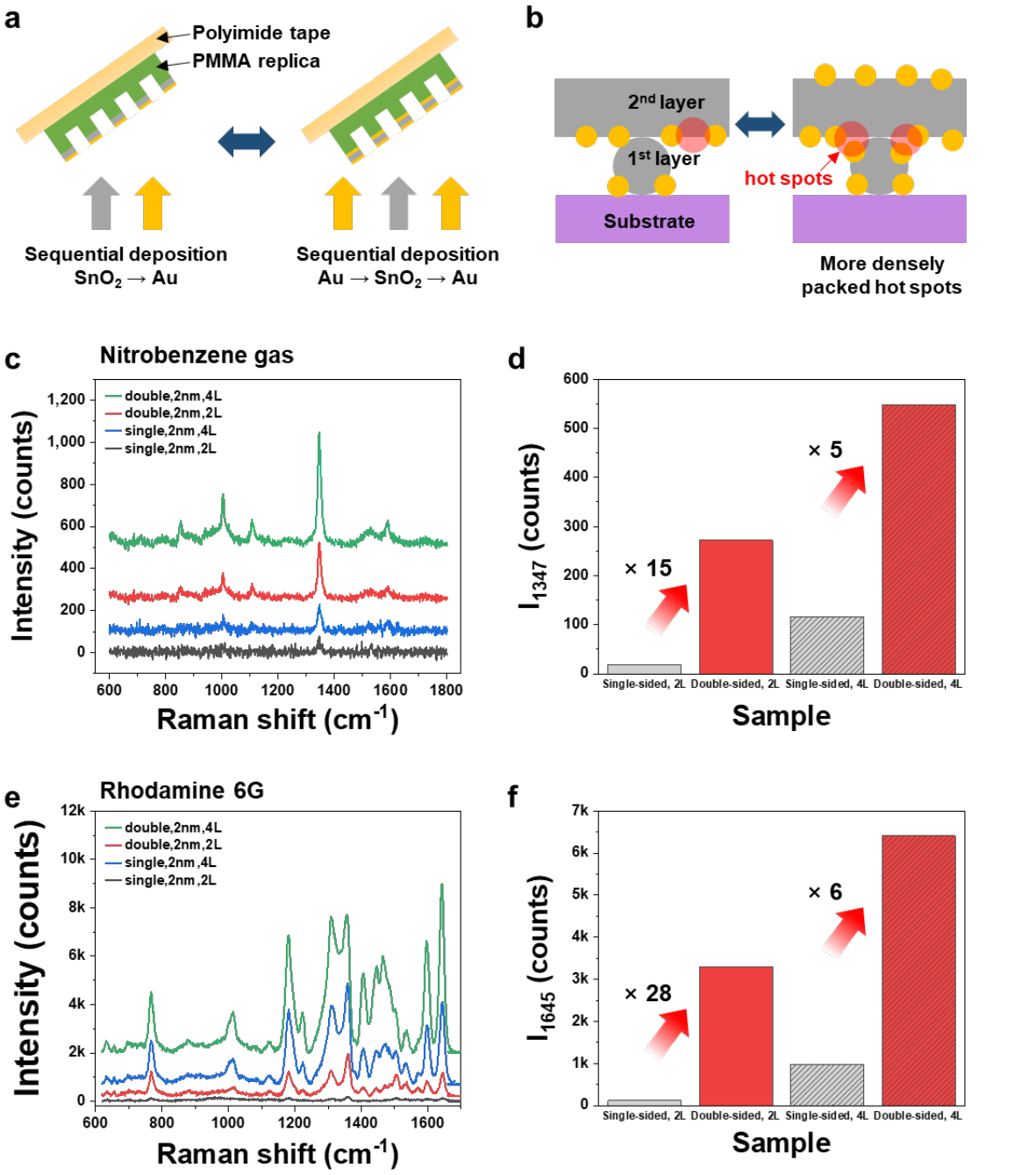

Figure S1. Effect of sandwich nanowire on SERS. a) Fabrication of single-sided Au-NP/SnO_2 and double-sided Au-NP/SnO_2/Au-NP. b) Schematic image of structural difference between single-sided Au-NP/SnO_2 and double-sided Au-NP/SnO_2/Au-NP. SERS spectra of c) nitrobenzene gas and e) R6G and SERS signal intensity at d) 1347 cm^{-1} for nitrobenzene and f) 1645 cm^{-1} for R6G obtained from 3D-CMA by varying the number of multi-stacking layers of single-sided Au-NP/SnO_2 and double-sided Au-NP/SnO_2/Au-NP.

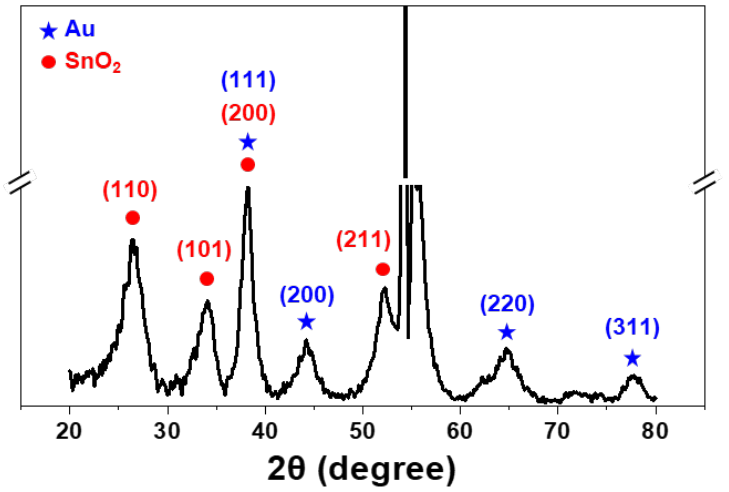

Figure S2. X-ray diffractometry analysis of 3D cross-point multifunctional architecture (3D-CMA). The theta-2 theta XRD scan clearly shows the pattern of the SnO_2 peak (red dot) and Au peak (blue star), respectively.

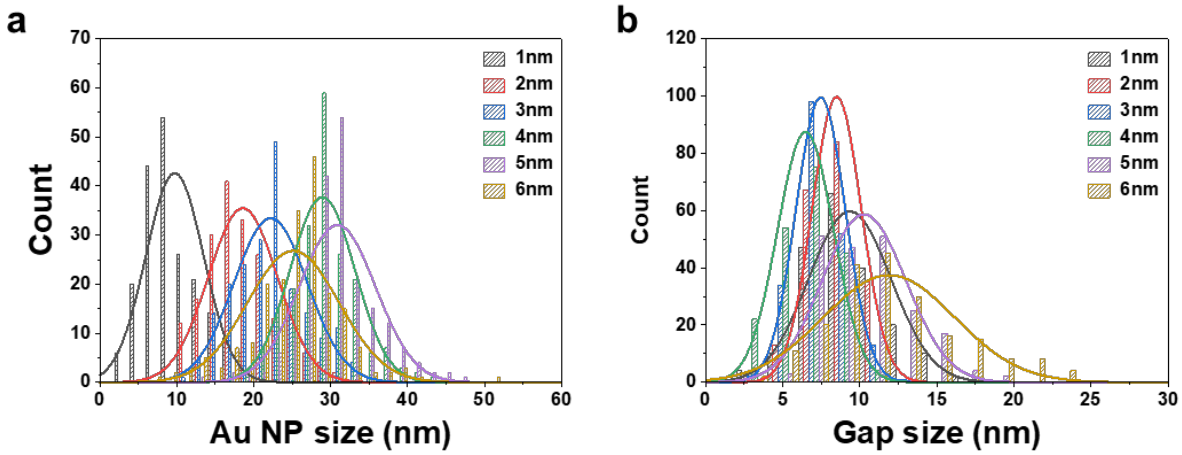

Figure S3. Distribution of a) Au NP size and b) interparticle gap size obtained from the SEM and TEM images of 1, 2, 3, 4, 5, 6 nm-deposited Au-NP/SnO_2/Au-NP nanowires.

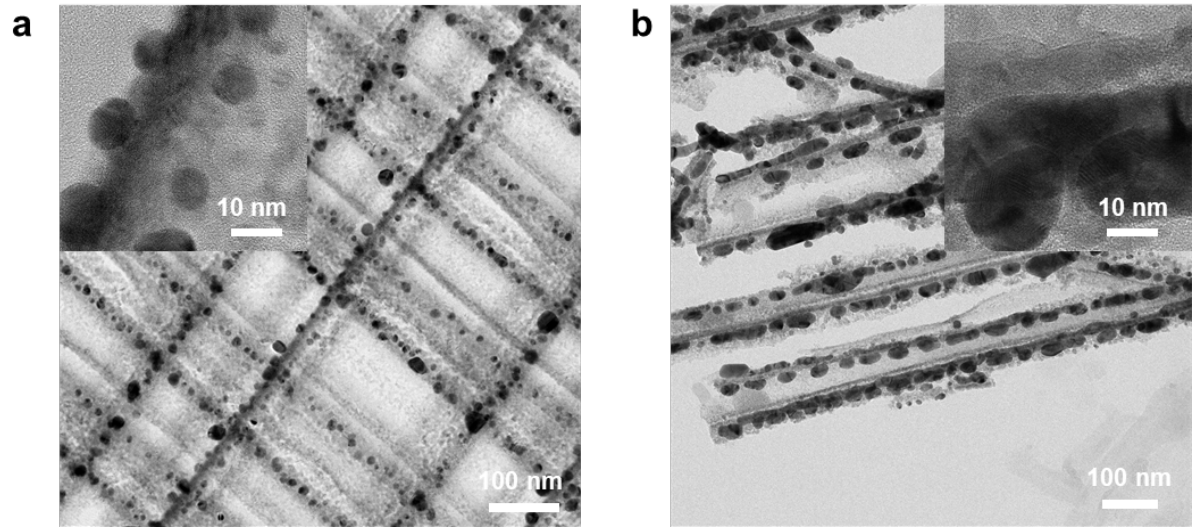

Figure S4. TEM images of a) 1 nm-deposited and b) 4 nm-deposited Au-NP/SnO_2/Au-NP after annealing

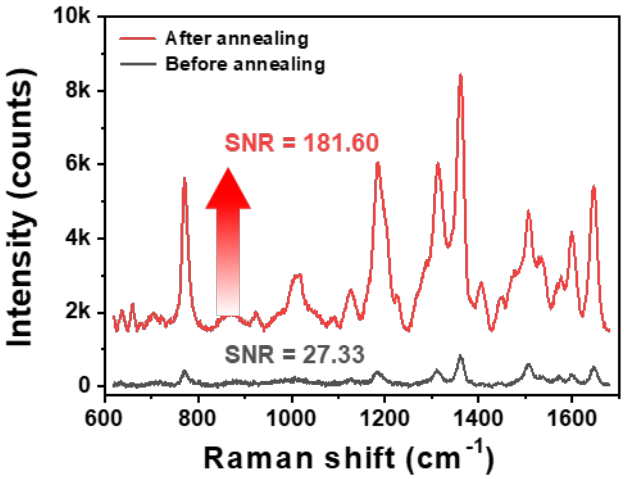

Figure S5. SERS spectra obtained from R6G-decorated 3D-CMA before and after annealing.

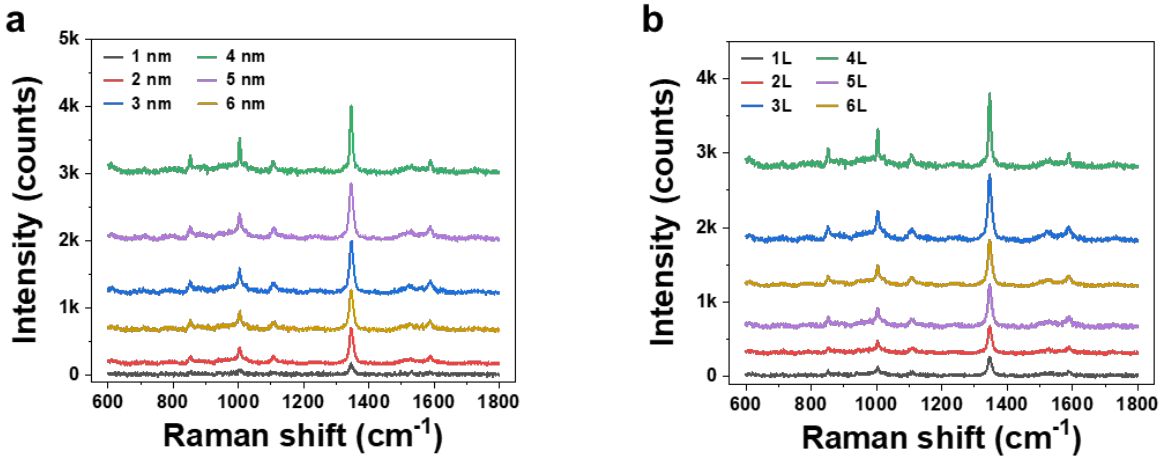

Figure S6. SERS spectra of nitrobenzene gas obtained from a) 4-layered 3D-CMA by varying Au deposition thickness and b) 4-nm deposited 3D-CMA by varying the number of multi-stacking layers.

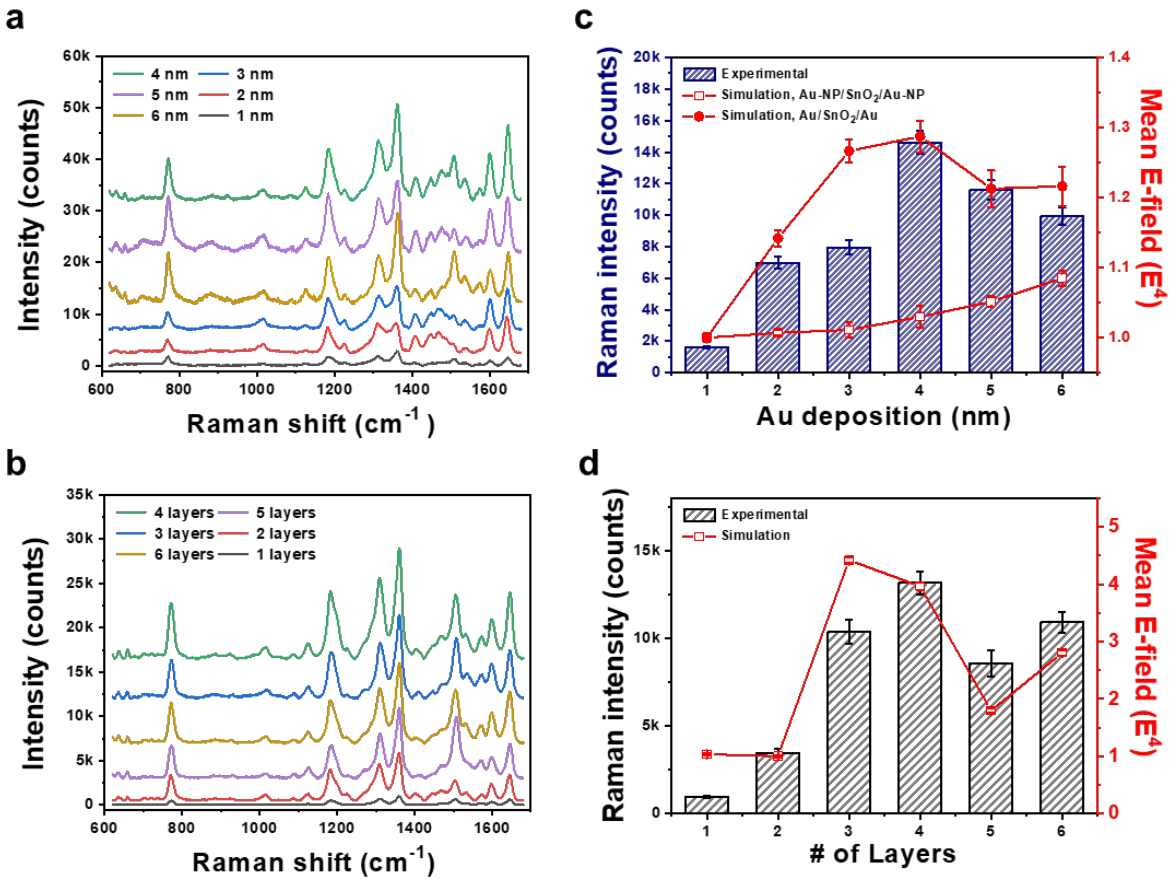

Figure S7. Experimental SERS spectra compared with E-field simulation results. SERS spectra of R6G obtained from a) 4-layered 3D-CMA by varying Au deposition thickness and b) 4-nm deposited 3D-CMA by varying the number of multi-stacking layers. c) For 4-layered 3D-CMA, measured SERS intensity of R6G taken from 1645 cm^{-1} (blue column) and calculated mean $|E/E_0|^4$ (red curves, solid squares for nanoparticles and empty squares for thin films) with respect to different Au deposition thicknesses. g) For 4-nm-Au-coated 3D-CMA, measure SERS intensity of R6G taken from 1645 cm^{-1} (black column) and calculated mean e-field (E^4) (red square) with respect to number of stacking layers.

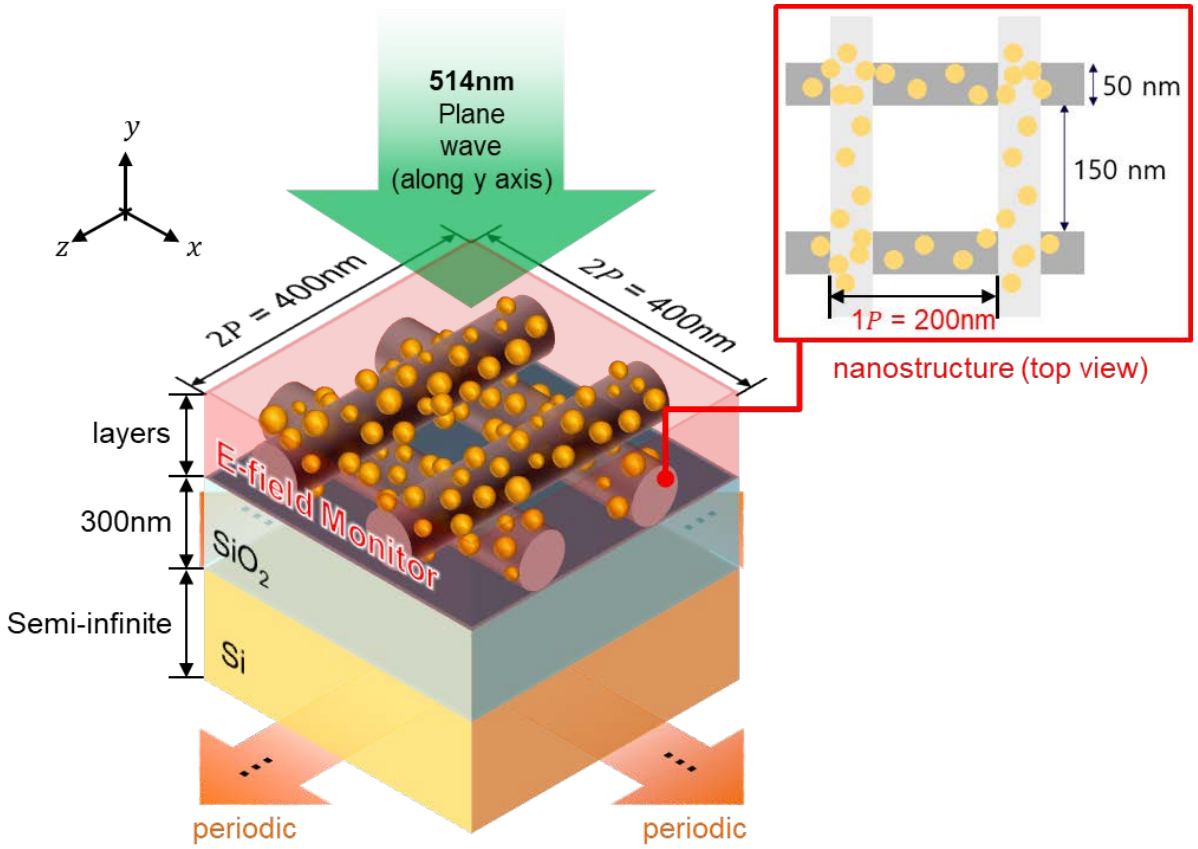

Figure S8. FDTD simulation model.

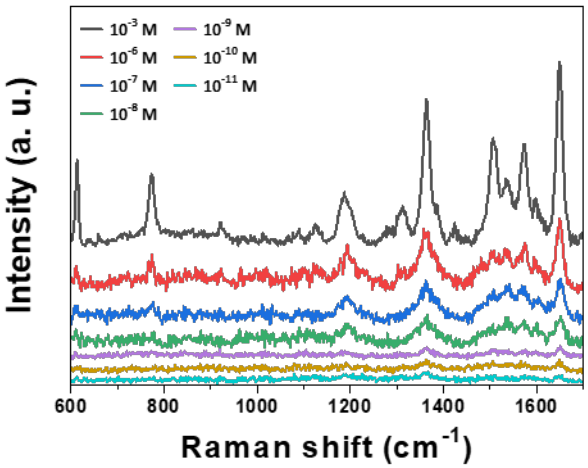

Figure S9. SERS spectra obtained from R6G concentrations from 10^{-3} M to 10^{-11} M

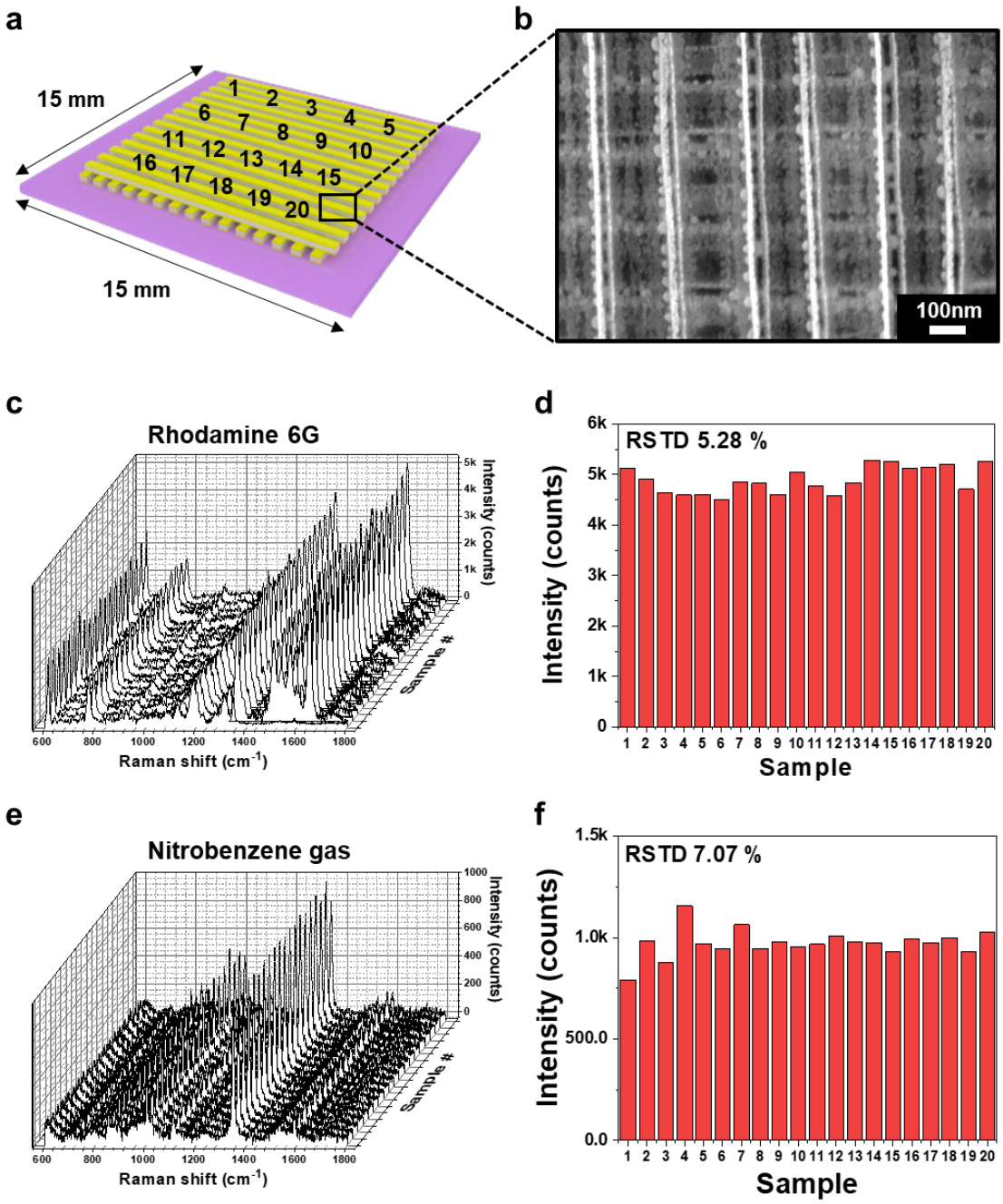

Figure S10. Point-to-point signal uniformity of 3D-CMA. SERS signals were obtained from 20 spots on the substrate. a) Schematic image of the large-area printed structure. The numbers represent the points where the SERS spectra were obtained. b) SEM image of 3D-CMA from one spot of the substrate. SERS spectra collected randomly from 20 spots for c) R6G and e) nitrobenzene gas and bar graphs representing the distribution of SERS intensities for d) R6G with a relative standard deviation of 5.28 % and f) nitrobenzene gas with a relative standard deviation of 7.07 %.

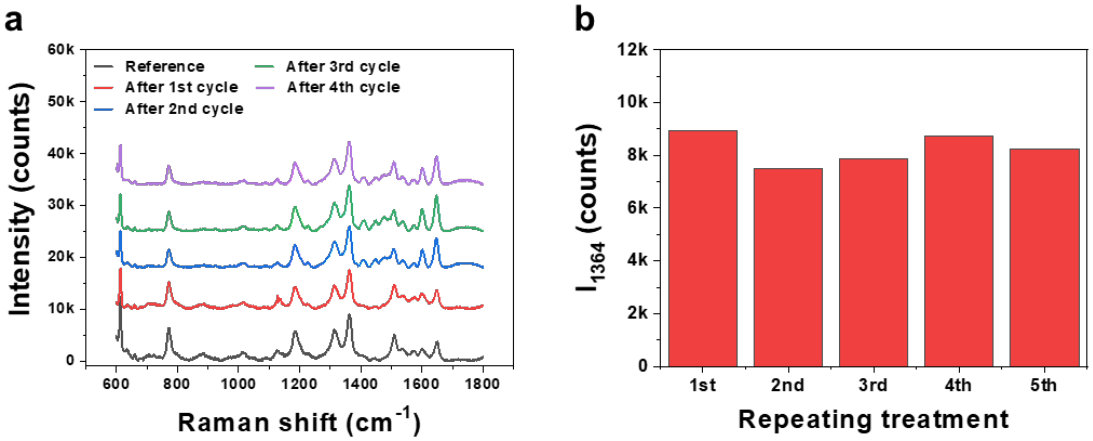

Figure S11. Thermal stability test. Thermal stability was confirmed via a thermal cycling test that repeated the SERS signal measurement with the same amount of R6G molecules drop-casted on the 3D-CMA after 500 ºC heat treatment for 1 h. The heat treatment also removes organic residues from the previous measurement. a) SERS signals obtained from R6G-decorated 3D-CMA with repeating thermal treatment at 500 °C for 1 h. b) A bar graph that shows the mean intensity at 1364 cm^{-1} of the characteristic SERS peaks of the R6G with repeating thermal treatment.

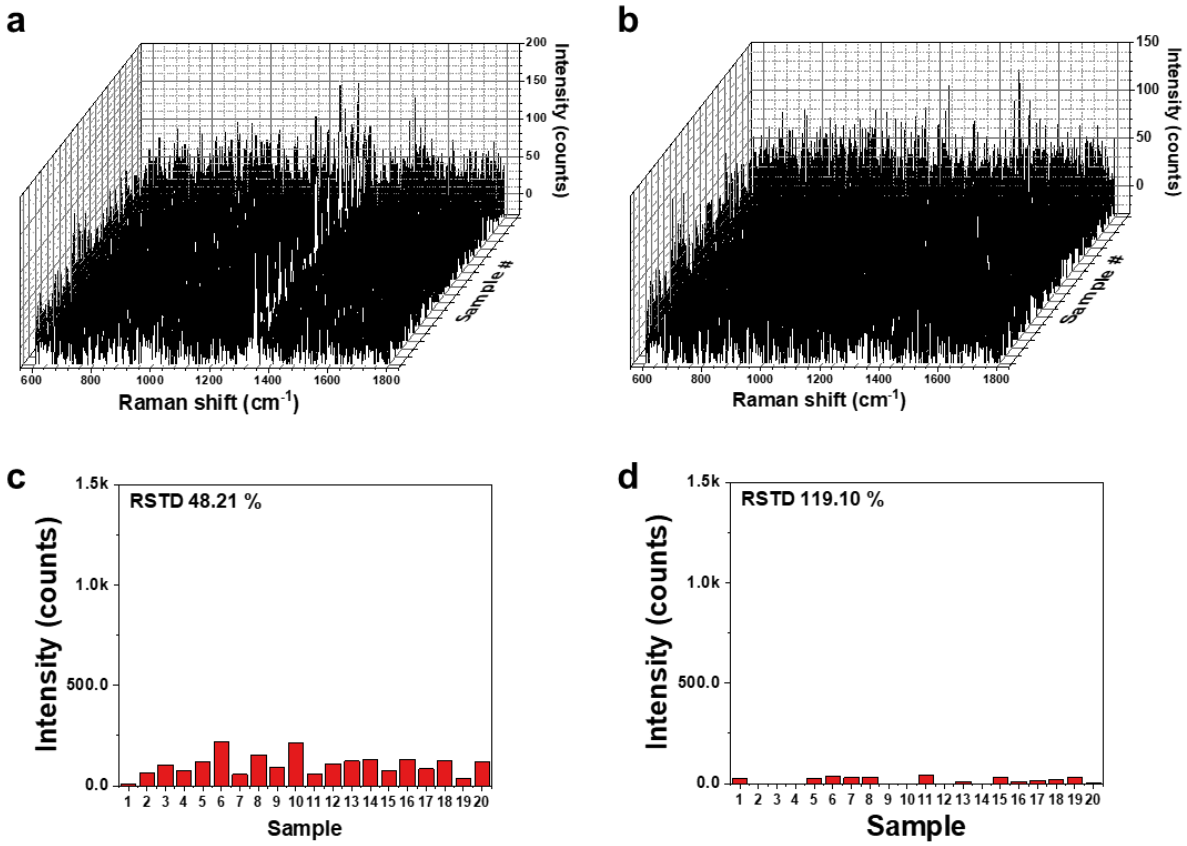

Figure S12. Point-to-point signal variation of a, c) disordered Au-NP/SnO_2/Au-NP and b, d) Au NP on SnO_2 film sample. 3D-CMA. Graph arrays showing point-to-point SERS spectra of nitrobenzene gas from a) disordered Au-NP/SnO_2/Au-NP and b) Au NP on SnO_2 film sample. Bar graphs representing the distribution of SERS intensities at 1347 cm^{-1} for c) disordered Au-NP/SnO_2/Au-NP with a relative standard deviation of 48.21 % and d) Au NP on SnO_2 film sample with a relative standard deviation of 119.10 %.

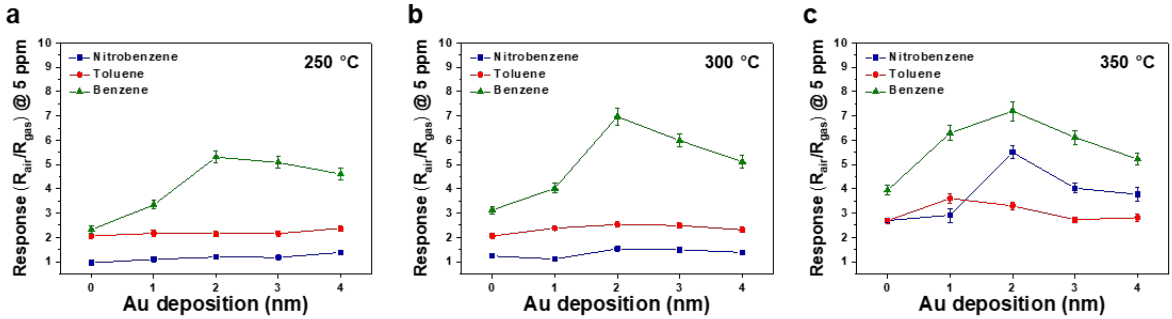

Figure S13. Dependence of gas sensing properties on deposition and temperature. Response at 5 ppm nitrobenzene, toluene, and benzene with varying Au deposition thickness at different temperature: a) 250 °C, b) 300 °C, and c) 350 °C, respectively.

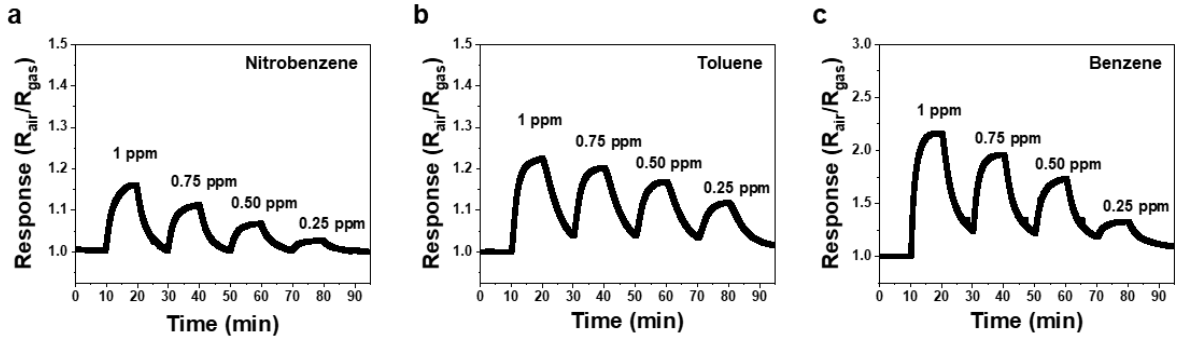

Figure S14. Dynamic gas sensing response curves obtained from 3D-CMA of a) nitrobenzene, b) toluene, and c) benzene for concentrations 1-0.25 ppm.

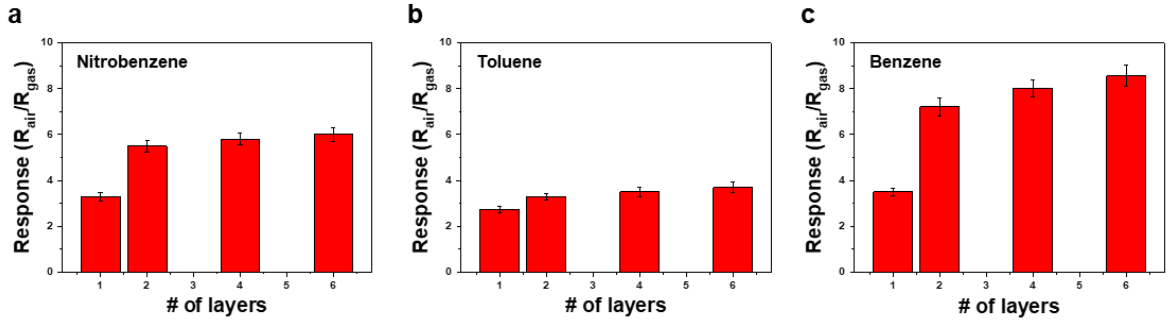

Figure S15. Dependence of gas sensing properties on number of multi-stacking layers obtained from 2 nm-deposited Au-NP/SnO_2/Au-NP nanowires measured at 350 °C for 5 ppm a) nitrobenzene, b) toluene, and c) benzene, respectively.

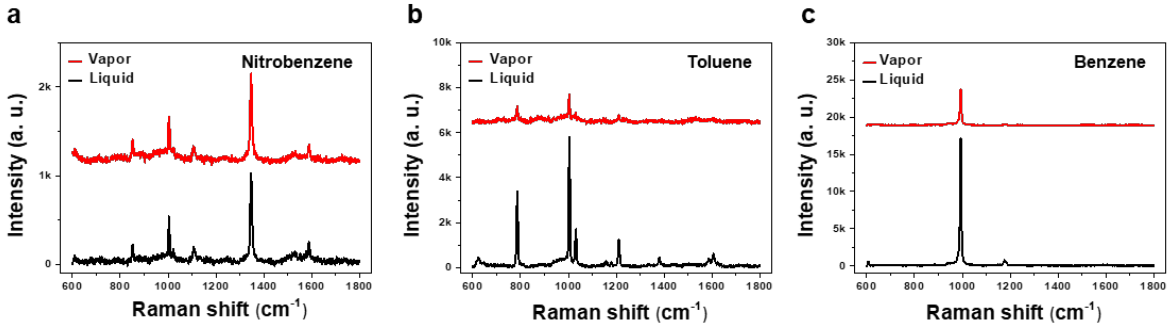

Figure S16. SERS spectra obtained with 3D-CMA from liquid and vapor phase a) nitrobenzene, b) toluene, and c) benzene.

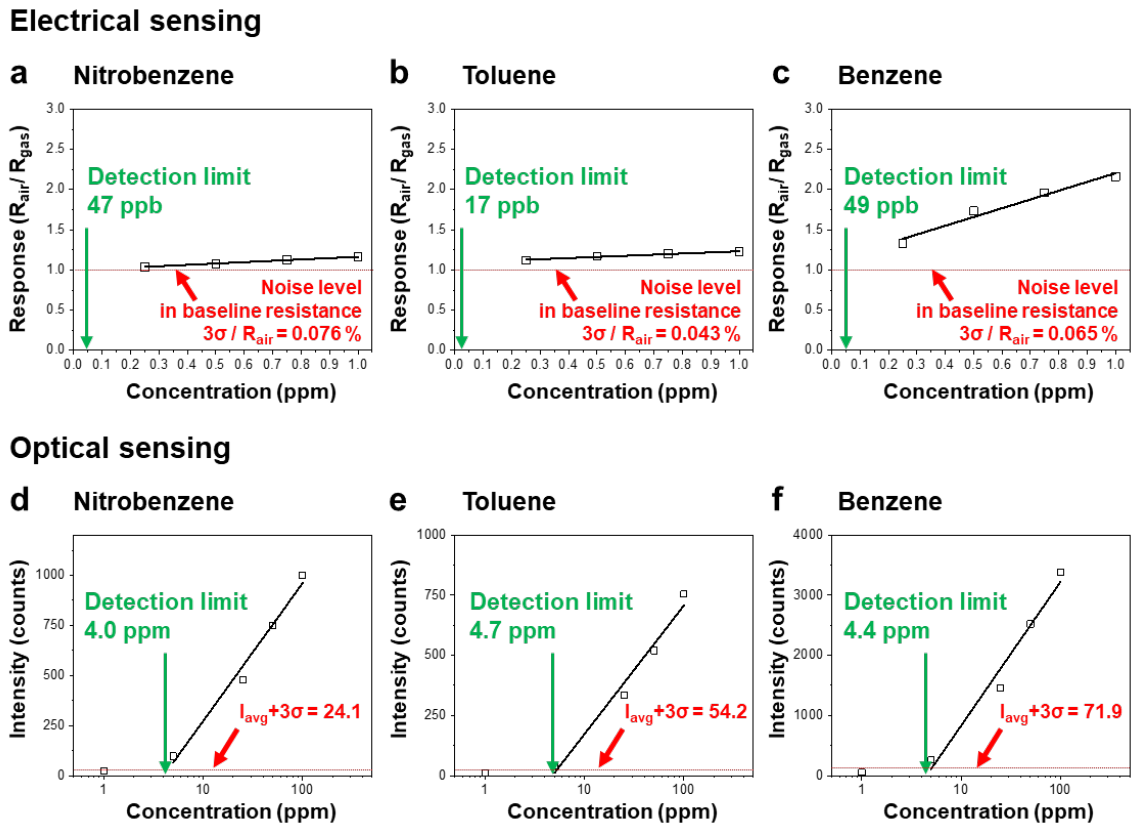

Figure S17. Limit of detection (LOD) calculations for a-c) electrical sensing and d-f) optical sensing component. Approximation from linear plot of sensor response and/or signal for a, d) nitrobenzene, b, e) toluene, and c, f) benzene. Characteristic Raman bands selected for analysis are 1347 cm^{-1} for nitrobenzene, 786 cm^{-1} for toluene, and 992 cm^{-1} for benzene.

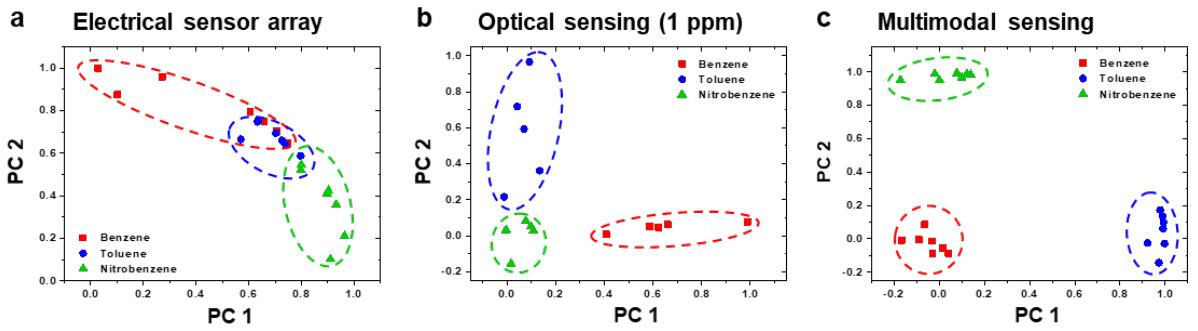

Figure S18. Discrimination of target gases with similar molecular structures (benzene, toluene, and nitrobenzene) by principal component analysis (PCA) using datasets from different sensor systems. a) PCA using electrical sensing results from an array of four metal oxide electrical gas sensors (SnO_2 nanowires, 1 nm Pt-decorated SnO_2 nanowires, and 3D-CMA with 2 nm- and 4 nm-deposited Au-NP/SnO_2/Au-NP). b) PCA using only the optical sensing results from 3D CMA (4-layer and 4 nm-deposited Au-NP/SnO_2/Au-NP) from target gases at concentrations of 1 ppm. c) PCA using electrical and optical multimodal sensing results from a single 3D-CMA multimodal sensor (4-layer and 4 nm-deposited Au-NP/SnO_2/Au-NP) from target gases at concentrations of 100-5 ppm. Whereas PCA from electrical sensing results show overlapping areas even with data collected by sensor arrays, PCA results from a single unit of the 3D-CMA multimodal sensor showed no overlapping areas, indicating clear discrimination of each target gas. This can be attributed to the optical sensing results in Figure 4g-i, which can differentiate each target gas even at concentrations as low as 1 ppm.

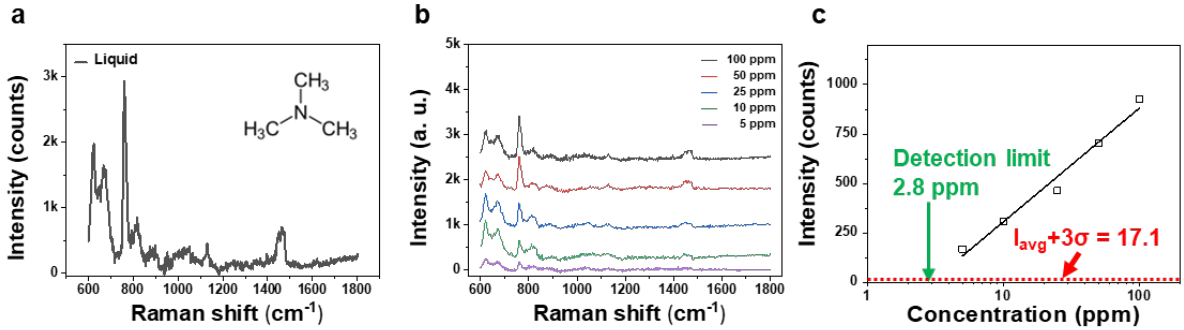

Figure S19. Demonstration of 3D-CMA as ppm-level gas sensor for food safety. SERS spectra from trimethylamine in a) liquid phase and b) gas phase at concentrations between 100 – 5 ppm. SERS intensity of the characteristic band at 760.4 cm^{-1} follows a linear relationship with the log of gas concentration. c) From the linear fitting of the SERS intensity change as a function of gas concentration, the LOD is calculated to be 2.8 ppm.

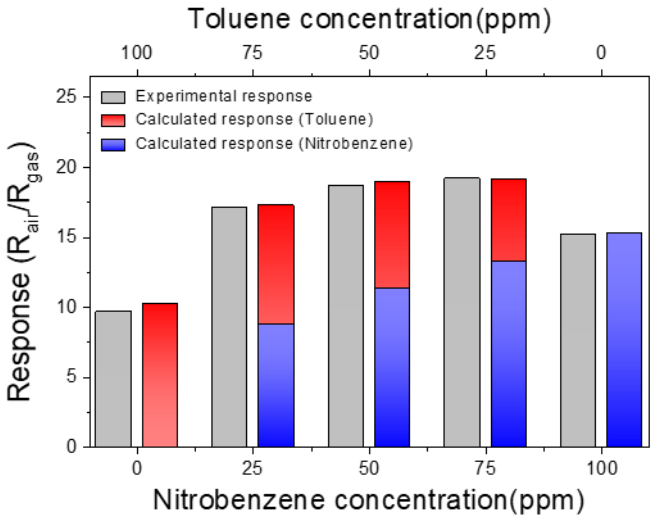

Figure S20. Comparison of experimental responses and calculated responses using single-component gas measurement data with variation of the ratio of the mixed gases.

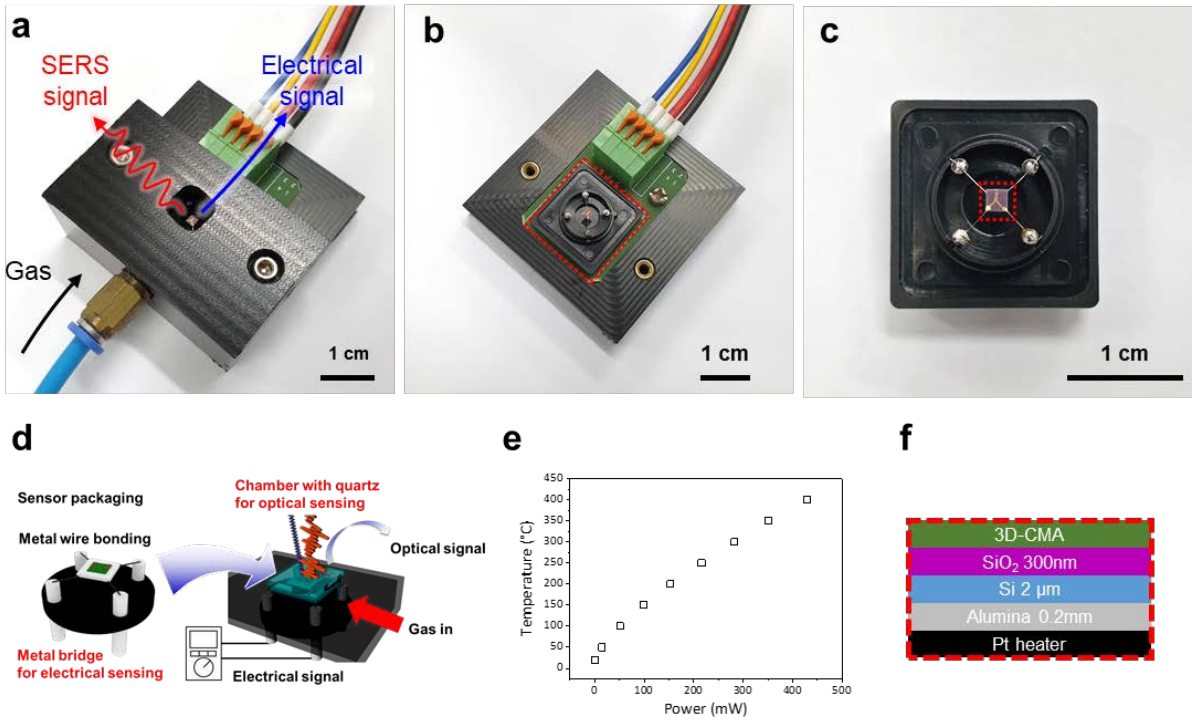

Figure S21. Images and specifications of the multimodal sensing platform. a) Photographic image of the a) exterior frame showing a top window for SERS signal collection, b) electrical components connect with c) the chip carrier wired with our 3D-CMA substrate. d) Schematic image of gas chamber and multimodal sensor packaging. e) Substrate temperature vs. applied power of the Pt heater on the substrate. Voltages of 0.53, 1.00, 1.47, 1.96, 2.46, 2.97, 3.49, 4.03, and 4.59 V were applied to the micro-heater to achieve operation temperatures of 50-450 °C, respectively. c) Photographs of multimodal sensor packaging with wire bonding. f) Schematic of the cross-section of multimodal sensor, marked as a red box in Figure S21c.

Table S1. Simulation information for nanoparticle size and distribution

Au deposition thickness [nm]	Au NP size [nm]	Gap size [nm]	Embedding depth [nm]
1	9.7 (± 4.0)	9.3 (± 4.6)	3.6
2	17.6 (± 3.6)	8.5 (± 1.8)	7.3
3	23.8 (± 3.8)	7.2 (± 2.1)	10.9
4	27.5 (± 4.8)	6.3 (± 1.9)	13.8
5	30.6 (± 5.3)	9.6 (± 3.1)	16.6
6	25.6 (± 7.9)	11.1 (± 5.0)	20.6

Embedding depth: In order to consider deformation effects that occur as the NP diameter increases, as shown in Figure S4, the embedding depth of the NP in the simulation increased. In particular, to simulate the experimental situation similarly, the embedded spheres are placed so that their height does not exceed 25 nm relative to the nanowire surface.

References

[1] J. W. Jeong, M. M. P. Arnob, K. M. Baek, S. Y. Lee, W. C. Shih, Y. S. Jung, *Adv. Mater.* **2016**, *28*, 8695.

[2] E. Le Ru, E. Blackie, M. Meyer, P. G. Etchegoin, *J. Phys. Chem. C* **2007**, *111*, 13794.

[3] X. Qiao, B. Su, C. Liu, Q. Song, D. Luo, G. Mo, T. Wang, *Adv. Mater.* **2018**, *30*, 1702275.

[4] K. M. Baek, J. Kim, S. Kim, S. H. Cho, M. S. Jang, J. Oh, Y. S. Jung, *Chem. Mater.* **2018**, *30*, 6183.

[5] L. Xu, W. Yan, W. Ma, H. Kuang, X. Wu, L. Liu, Y. Zhao, L. Wang, C. Xu, *Adv. Mater.* **2015**, *27*, 1706.

[6] D. Zhang, L. Huang, B. Liu, H. Ni, L. Sun, E. Su, H. Chen, Z. Gu, X. Zhao, *Biosens. Bioelectron.* **2018**, *106*, 204.

[7] C. Hierold, R. Müller, *Sensors and Actuators* **1989**, *17*, 587.

[8] K.-M. Park, T.-W. Kim, J.-H. Park, C.-O. Park, *Sensor Actuat. B-Chem.* **2017**, *239*, 841.

[9] N. Yamazoe, G. Sakai, K. Shimanoe, *Catal. Surv. Asia* **2003**, *7*, 63.